The Pisces Plume and the Magellanic wake

Vasily Belokurov [ORCID],[1,2]★ Alis J. Deason [ORCID],[3] Denis Erkal [ORCID],[4] Sergey E. Koposov [ORCID],[1,5] Julio A. Carballo-Bello,[6,7] Martin C Smith,[8] Prashin Jethwa [ORCID][9] and Camila Navarrete [ORCID][6,10,11]

[1]*Institute of Astronomy, Madingley Rd, Cambridge CB3 0HA, UK*
[2]*Center for Computational Astrophysics, Flatiron Institute, 162 5th Avenue, New York, NY 10010, USA*
[3]*Institute for Computational Cosmology, Department of Physics, University of Durham, South Road, Durham DH1 3LE, UK*
[4]*Department of Physics, University of Surrey, Guildford GU2 7XH, UK*
[5]*Department of Physics, McWilliams Center for Cosmology, Carnegie Mellon University, 5000 Forbes Avenue, Pittsburgh, PA 15213, USA*
[6]*Instituto de Astrofísica, Pontificia Universidad Católica de Chile, Av. Vicuña Mackenna 4860, 782-0436 Macul, Santiago, Chile*
[7]*Chinese Academy of Sciences South America Center for Astronomy, National Astronomical Observatories, CAS, Beijing 10010, People's Republic of China*
[8]*Key Laboratory for Research in Galaxies and Cosmology, Shanghai Astronomical Observatory, Chinese Academy of Sciences, 80 Nandan Road, Shanghai 200030, People's Republic of China*
[9]*European Southern Observatory, Karl-Schwarzschild-Str 2, D-85748 Garching, Germany*
[10]*Millennium Institute of Astrophysics, Av. Vicuña Mackenna 4860, 782-0436 Macul, Santiago, Chile*
[11]*European Southern Observatory, Alonso de Córdova 3107, 7630000 Vitacura, Santiago, Chile*

ABSTRACT

Using RR Lyrae stars in the *Gaia* Data Release 2 and Pan-STARRS1 we study the properties of the Pisces overdensity, a diffuse substructure in the outer halo of the Milky Way. We show that along the line of sight, Pisces appears as a broad and long plume of stars stretching from 40 to 110 kpc with a steep distance gradient. On the sky Pisces's elongated shape is aligned with the Magellanic Stream. Using follow-up VLT FORS2 spectroscopy, we have measured the velocity distribution of the Pisces candidate member stars and have shown it to be as broad as that of the Galactic halo but offset to negative velocities. Using a suite of numerical simulations, we demonstrate that the structure has many properties in common with the predicted behaviour of the Magellanic wake, i.e. the Galactic halo overdensity induced by the infall of the Magellanic Clouds.

Key words: stars: variables: RR Lyrae – galaxies: dwarf – Local Group – Magellanic Clouds – galaxies: structure.

1 INTRODUCTION

The implications of the arrival of a massive (see e.g. Peñarrubia et al. 2016) Large Magellanic Cloud (LMC) on a highly eccentric and rapidly evolving orbit (Besla et al. 2007; Kallivayalil et al. 2013) are many fold. First, in response to the interaction with a massive satellite, the barycentre of the Milky Way should move (Gómez et al. 2015), imprinting noticeable velocity gradients throughout the Galaxy (Erkal et al. 2018). Second, the MC fly-by will violently disturb the Galactic disc (both stellar and gaseous), warping and heating it out of equilibrium (Laporte et al. 2018). Finally, the giant satellite will gravitationally focus dark matter particles directly behind it, as it sinks to the centre of the Milky Way due to dynamical friction (Garavito-Camargo et al. 2019). This large-scale 'wake' ought to have an observable stellar counterpart, composed of MW halo stars at distances beyond ∼40 kpc.

In this letter, we explore the structure of the Galactic stellar halo at distances beyond ∼40 kpc from the Sun using a large sample of RR Lyrae provided by the *Gaia* Data Release 2 (Clementini et al. 2019; Holl et al. 2018) as well as the Pan-STARRS1 survey (PS1, Sesar et al. 2017). We show that the structure known as the Pisces overdensity is in fact a part of a long, broad, and nearly radial stream, which extends from ∼40 to >100 kpc in distance. Pisces was discovered as an overdensity of RR Lyrae stars with heliocentric distances ∼80 kpc in the SDSS Stripe 82 data (Sesar et al. 2007; Watkins et al. 2009), which provided only a limited view of the cloud. Most recently, Nie et al. (2015) used a large sample of photometrically selected blue horizontal branch (BHB) stars to map out the full extent of the Pisces structure. This expanded view revealed that rather than a cloud, the Pisces overdensity (i) shows a steep distance gradient and (ii) has a clearly elongated shape on the sky. Here we revisit the position and the highly stretched 3D structure of Pisces. Additionally, we collect and analyse kinematical information along a sightline through the overdensity. Our velocity measurements complement those obtained by Kollmeier et al.

★ E-mail: vasily@ast.cam.ac.uk

(2009) and Sesar et al. (2010) who found two groups of stars, one moving towards us and one away. We conclude by comparing the observed data to a theoretical expectation of the stellar wake forming in the halo as the LMC falls into the Galaxy.

2 PISCES PLUME WITH *GAIA* DR2 AND PS1 RR LYRAE

The analysis presented here is based on the combined sample of RR Lyrae stars of ab type, with the bulk of the data coming from the *Gaia* DR2, augmented by the RR Lyrae identified in the Pan-STARRS1 (PS1) survey by Sesar et al. (2017). More precisely, from the *Gaia* DR2 we select RR Lyrae candidates (see Clementini et al. 2019; Holl et al. 2018) with BP/RP excess factor (the ratio of the sum of the integrated BP- and RP-band flux and the *G*-band flux obtained via LSF/PSF fitting) less than 1.5, located in the areas of the sky with low or moderate dust reddening i.e. $E(B - V) < 0.7$. To clarify, the *Gaia* DR2 RR Lyrae rely on both the results of the general variability analysis (e.g. `vari_classifier_result` and `vari_time_series_statistics` tables) and the SOS (Specific Object Studies) analysis (`vari_rrlyrae` table). In short, our *Gaia* selection is similar to that discussed in Iorio & Belokurov (2019). From the PS1 data set Sesar et al. (2017), we select the most likely RR Lyrae candidates by applying a cut on *ab score* (a statistic akin to the probability of being an RR Lyrae star) above 0.8. Finally, we exclude objects in the central portion of the Galactic disc, i.e. those with $|l| < 120°$, $-14° < b < 12°$. The combination of above cuts yields a sample with a total of $\sim 98\,000$ RR Lyrae, of which some ~ 4000 are from the PS1.

Fig. 1 shows the density of GDR2 + PS1 RR Lyrae with Galactocentric distances between $R = 60$ and $R = 100$ kpc in equatorial coordinates. As evidenced in the figure, the distant halo of the Milky Way is dominated by three prominent overdensities. The largest of these, at RA $\sim 130°$ is associated with the Sgr stream, more precisely with its trailing tail apocentre. The red dashed lines mark the Sgr stream track, as approximated by a great circle with a pole at (RA, Dec.) = $(283.750°, -30.483°)$. The lines correspond to the stream-aligned latitudes $B_\odot = -10°$ and $B_\odot = 10°$ (see Belokurov et al. 2014, for details). The structure at RA $= -140°$, the so-called Outer Virgo Overdensity (OVO), lies beyond the apocentre of the stream's leading tail and may or may not be connected to the Sgr dwarf disruption (see Hernitschek et al. 2017; Sesar et al. 2017). The lower edge of the third overdensity, at RA $\sim -10°$ appears to overlap with the Sgr stream track. However, the whole structure extends much further, at least $\sim 20°$ out of the Sgr plane. Moreover, there is no simple way to link this material to the other known portions of the Sgr stream. Both the observations and the available models agree: the Sgr stream at this position on the sky is at $D < 30$ kpc.

The structure at RA $\sim -10°$ coincides with the previously reported detections of the so-called Pisces overdensity (Sesar et al. 2007; Watkins et al. 2009). The distances also broadly agree: the RR Lyrae displayed here are at D > 60 kpc, while the Pisces structure is at ~ 80 kpc. Strikingly, as the solid blue lines in Fig. 1 indicate, Pisces lies very close to the equator of the Magellanic Stream (MS). The MS coordinate system is suggested by Nidever, Majewski & Butler Burton (2008) and is supposed to be aligned with the Magellanic H I stream. The blue lines correspond to the MS-aligned latitudes $B_{MS} = \pm 15°$. Not only is Pisces located at the point of crossing of the Sgr and Magellanic streams, its shape appears to be stretched along the MS. The fact that on the sky the Pisces projected density distribution shows a clear preferred

direction has been noticed before. Namely, Nie et al. (2015) built the first comprehensive map of Pisces using BHB stars selected from the deep *u*-band imaging survey SCUSS and found a great circle aligned with the structure's elongation. The orientation of this great circle is shown in Fig. 1 with a black arrow. Clearly, the Pisces elongation as traced by Nie et al. (2015) deviates only slightly from the track of the MS. Note that the Pisces morphology shown in Fig. 1 may bear some signs of selection biases inherent to the GDR2 and PS1 data sets. In particular, the GDR2 RR Lyrae selection at faint magnitudes depends sensitively on the number of *Gaia* scans, distributed in a highly non-uniform fashion across the sky. Reassuringly however, for Dec. $> -10°$, the shape of the structure traced with RR Lyrae agrees well with that mapped using the BHBs, thus at these latitudes the effects of the *Gaia* scanning law may be minimal. At lower Dec., we expect a more serious selection bias: the BHB study of Nie et al. (2015) is limited to Dec. $> -10°$, while the PS1 sample does not reach below Dec. $= -30°$.

The right-hand panels of Fig. 1 show the galactocentric distance distribution of GDR2 + PS1 RR Lyrae as a function of the Sgr's longitude $\tilde{\Lambda}_\odot$ for two ranges of Sgr's latitude $\tilde{B}_\odot$. In these panels, the Pisces overdensity appears as a nearly vertical plume of stars, stretching from ~ 40 to beyond 100 kpc at around $\tilde{\Lambda}_\odot \sim 300°$. As indicated by the red dashed lines, the steep distance gradient apparent in the RR Lyrae distribution is consistent with that previously measured using the SCUSS BHBs by Nie et al. (2015). On comparing the two right-hand panels of the figure, it is apparent that the distribution of the RR Lyrae along the line of sight changes slightly as a function of $\tilde{B}_\odot$. At high $\tilde{B}_\odot$ (second panel) the Pisces Plume is the only significant substructure in the outer MW halo. Within the Sgr orbital plane (third panel), the dwarf's trailing tail becomes clearly visible, dropping from $r \sim 60$ kpc at $\tilde{\Lambda}_\odot \sim 200°$ to ~ 20 kpc at $\tilde{\Lambda}_\odot \sim 300°$. Curiously, apart from the Pisces Plume itself (mostly limited to $300° < \tilde{\Lambda}_\odot < 320°$), there is a narrow and nearly vertical stream at $\tilde{\Lambda}_\odot \sim 330°$. Given the position on the sky and the distance gradient (and as indicated with the small red filled circles), at least some of this additional signal can be attributed to the Orphan Stream (OS), which has recently been detected in this area of the sky (see Koposov et al. 2019). Note that, as shown by solid black lines in the left-hand panel of Fig. 1, the OS is much narrower than either the Sgr stream or the Pisces Plume.

3 PISCES PLUME WITH SUBARU HSC AND VLT FORS2

Recently, Deason, Belokurov & Koposov (2018) used the deep multiband photometry acquired as part of the Subaru Hyper Suprime-Cam (HSC) survey to select candidate BHB and Blue Straggler (BS) stars at large distances from the Sun. Once completed, the HSC survey will provide one of the deepest views of a large portion of the Milky Way halo. The subset of the data available currently is limited to seven fields with a combined area of ~ 100 deg^2. Deason et al. (2018) used a combination of *griz* filters to identify BHB and BS stars beyond 50 kpc and as far as 200 kpc. They point out that out of the seven fields considered in their analysis, three stand out clearly as they contain a significantly larger number of distant tracers. Two of these are projected on to the Sgr stellar stream, the likely source of contamination. They argue that the third overdense HSC field, namely VVDS, lies close to the equator of the MS coordinate system (see Fig. 1) and therefore may be related to the Magellanic Clouds. As the figure indicates, the VVDS field also overlaps with the overdensity of PS1 + GDR2 RR Lyrae associated with the Pisces Plume.
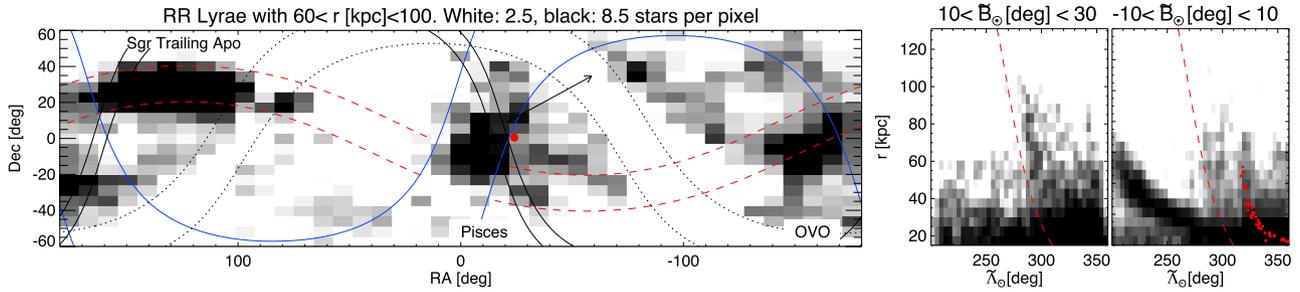
Figure 1. *Left:* Density of distant GDR2 + PS1 RR Lyrae candidates in equatorial coordinates. Stars as close as ∼60 kpc and as far as ∼100 kpc are included. Three obvious overdensities are visible: the apocentric pile-up of the Sgr dsph trailing debris at $90° < RA < 160°$, the Outer Virgo Overdensity (OVO) at $−180° < RA < −140°$, and the Pisces cloud of stars at $−30° < RA < 10°$. The solid blue lines indicate the region within the Magellanic Stream, i.e. $−15° < B_{MS} < 15°$. The red dashed lines give the Sgr stream track, i.e. $−10° < \tilde{B}_{\odot} < 10°$. The solid black lines are offset $±3°$ from the Orphan Stream track. The Galactic plane ($b = ±10°$) is marked with dotted black lines. The black arrow is the direction of the Pisces elongation as measured by Nie et al. (2015). The filled red circle marks the location of the HSC's VVDS field. *Right:* Heliocentric distance distribution of the GDR2 + PS1 RR Lyrae as a function of Sgr's longitude $\tilde{\Lambda}_{\odot}$ for two different ranges of Sgr's latitude $\tilde{B}_{\odot}$. The Pisces distance gradient estimated by Nie et al. (2015) using SCUSS BHBs is shown as a red dashed line (offset by $−15°$ from their central location). The small red filled circles are the OS RR Lyrae from Koposov et al. (2019) with $\tilde{B}_{\odot} < 10°$.

3.1 Spectroscopic follow-up with VLT/FORS2

To explore the VVDS overdensity further, we performed spectroscopic follow-up of BHB candidates in the VVDS field with VLT/FORS2. The candidates were selected from the HSC data, with $0.0 < griz < 0.07$, where $griz = i − z − 0.3(g − r) + 0.035$. Our original target list had $N = 19$ candidates, but after inspection of the *Gaia* DR2 astrometry of the relatively bright candidates ($g < 20$), we found that two of these were obvious white dwarfs (with large proper motions). Our observations were taken over four half nights in visitor mode from 2018 October 6 to 2018 October 10 (PI:Deason, ID:0102.B-0029(A)) using the FORS2 spectrograph. The instrument was used in long-slit mode with the E2V detector, SR collimator, a binning of $2 × 2$, and a 1.0 arcsec slit. We used the 1200B + 97 grism, with a dispersion of 0.36 Å per pixel. The wavelength range provided by this configuration spans 3600–5110 Å. Our targets spanned a magnitude range of $20 < g < 21.5$, and the exposure times ranged from 20 min to 2 h depending on the apparent magnitude and weather conditions. Data were taken for 17 targets during our observing run. 15 of these had good data (S/N >10), while two faint targets (with $g > 21$) had insufficient signal-to-noise (S/N ≪10). We also observed four bright BHB/BS stars from the Xue et al. (2011) catalogue. These were used to test our separation of BHB and BS stars, and evaluate our velocity precision. The data were reduced using the standard ESO pipelines using the ESOREX package. These procedures included bias-subtraction, flat-fielding correction, spectral extraction, sky correction, and wavelength calibration.

3.2 Radial velocities and A-type star classification

We fit Sersic profiles to the $H\alpha$, $H\gamma$, and $H\beta$ Balmer lines (see Navarrete et al. 2019 equation 1), and the radial velocities are calculated by fitting all three lines simultaneously. The models are convolved with a Gaussian with FWHM = 2.88 Å (corresponding to 4 pixels). The errors on the derived velocities include the fitting errors and the wavelength calibration uncertainty (∼0.15 pix). An additional source of uncertainty is the offset in the centring of the star in the slit. Using repeat measurements, and standard BHB/BS stars, we estimate that this additional error source can reach up to ∼10 km s^{-1}. However, we do not include this error in our analysis,

as this is an upper bound and each star would have a slightly different offset.

In order to separate BHB and BS stars, we use the Sersic profile of the $H\gamma$ line, which we found to be the most discerning (cf. Clewley et al. 2002). In the left-hand panel of Fig. 2 we show the b_γ and c_γ Sersic indices for our A-type stars. The star symbols show the four A-type stars from Xue et al. (2011). The BHB and BS stars are clearly separated in this plane, and the confirmed BHB/BS stars are shown in blue/red. The velocity distribution of these stars is shown in the middle-left panel. When converting to Galactocentric velocities, both barycentric and heliocentric corrections are applied, and we assume the solar velocity is $(V_x, V_y, V_z) = (11.1, 12.24 + 235, 7.25)$ km s^{-1}. The velocity distribution of the BHB stars is broad, but with a bias towards negative velocities: $(\sigma(v_{gsr}), \langle v_{gsr} \rangle) = (118^{+35}_{-24}, −57^{+39}_{-39})$ km s^{-1}. The middle-right panel shows the Galactocentric velocity as a function of distance. We assign distances to the BHB and BS stars using the relations given in Deason, Belokurov & Evans (2011). Here, we can again see that the BHB stars in the radial range 40–80 kpc have a broad velocity distribution, and are biased towards negative values.

To further investigate these stars in the VVDS field, we estimate their metallicities ([Fe/H]) using the equivalent width of the Ca II K line at 3933 Å. We adopt the relations derived in Navarrete et al. (2019). For consistency, we check that our estimated metallicities agree with the SDSS SEGUE metallicities for the known BHB/BS stars: we find that they all agree within 1σ. The resulting [Fe/H] values are shown in the right-hand panel of Fig. 2 against velocity. Here, we can see no obvious chemical signature and the BHB stars appear to have metallicities typical of 'field' halo stars, with [Fe/H] ∼ −2.0. In summary, the excess of BHB stars in the VVDS field have a broad velocity distribution, with a (∼1.5σ significance) bias towards negative radial velocities. Moreover, these stars have metallicities consistent with the field halo population.

4 DISCUSSION AND CONCLUSIONS

4.1 Comparison to simulations

Although the plume in Fig. 1 appears somewhat stream-like, the radial velocities in Fig. 2 do not reveal any obvious cold components. Instead, they show a dispersion consistent with that
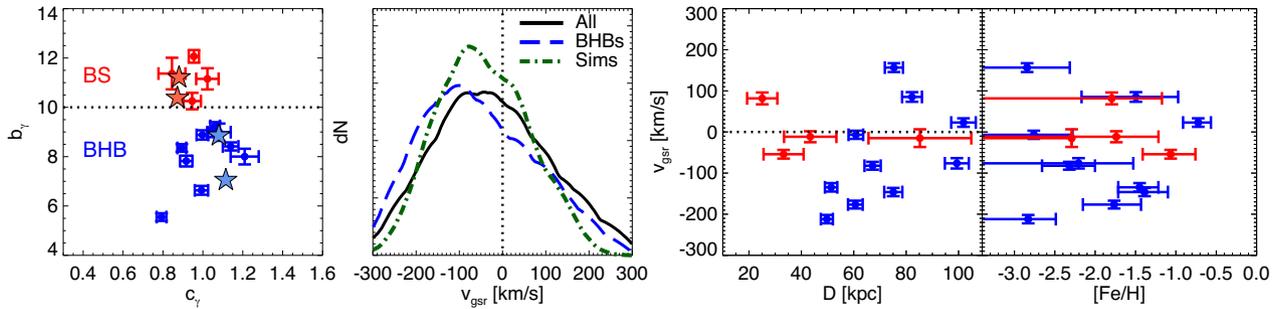
Figure 2. *Left:* Sersic profile parameters for the Hγ Balmer line, c_γ, b_γ. BHB stars are shown in blue and BS stars are shown in red. The star symbols indicate the known BHB/BS stars from the Xue et al. (2011) SDSS sample. The BHB and BS stars separate at $b_\gamma \sim 10$. *Middle-left:* The line-of-sight velocity distribution of the A-type stars in Galactocentric coordinates. The black line is for all A-type stars, the dashed blue line indicates the BHB star distribution, and the dot–dashed green line shows the velocity distribution from a simulated stellar halo affected by the LMC's infall (see Section 4.1). The BHB stars have a broad distribution, with a bias towards negative radial velocities, in good agreement with the simulations. *Middle-right:* Line-of-sight velocity against distance. The BHB stars in the distance range $40 < D_{BHB}/kpc < 80$ have negative radial velocities. *Right:* Line-of-sight velocity against metallicity. The stars in the VVDS field have similar metallicities to the 'field' halo population.

of the MW's stellar halo (e.g. Bird et al. 2019; Lancaster et al. 2019) with a slight bias towards negative line-of-sight velocities. Interestingly, such a shift in the stellar halo's velocity was predicted in Erkal et al. (2018) who argued that the LMC's infall should induce a substantial reflex motion in the inner regions of the Milky Way relative to its outskirts. This effect would push the mean radial velocity of the stellar halo in the Pisces region to be negative. This effect was also seen in Garavito-Camargo et al. (2019) who simulated the LMC's infall and found that it should also induce a substantial wake, i.e. overdensity, in the Milky Way's stellar halo.

In order to test this prediction, we evolve the Milky Way in the presence of various mass LMCs. This is done using a similar set-up as Erkal et al. (2018). Crucially, the Milky Way is treated as a particle sourcing the `MWPotential2014` from Bovy (2015) where we have replaced the bulge with a Hernquist bulge with a mass of 5×10^9 M$_\odot$ and a scale radius of 500 pc for computational efficiency. This allows the Milky Way to respond to the LMC's infall which is essential for correctly capturing the LMC's full effect. The LMC is modelled with a Hernquist profile with a mass of $[2, 5, 10, 15, 20, 25] \times 10^{10}$ M$_\odot$. For each LMC mass, we fix the scale radius by requiring the circular velocity at 8.7 kpc matches the observed value of 91.7 km s^{-1} from van der Marel & Kallivayalil (2014). The stellar halo is set up in equilibrium using AGAMA (Vasiliev 2019). Namely, we use the `DoublePowerLaw` distribution function which is similar to the two-power models described in section 3 of Posti et al. (2015). We use `norm = 1.5e10`, `j0 = 500`, `slopeIn = 0`, `slopeOut = 3.5`, `coefJrOut = 0.75`, `coefJzOut = 1.125`, `jcutoff = 1e5`, `cutoffStrength = 2`. This produces a nearly spherical stellar halo with an outer power-law slope of -3.2 beyond $\sim$20 kpc, and an almost constant anisotropy of 0.475 between 10 and 500 kpc. This broadly resembles the observed stellar halo's properties, albeit with a slightly shallower density fall off (e.g. Deason et al. 2011) and a constant instead of falling anisotropy (e.g. Bird et al. 2019). We sample this stellar halo with 10^7 particles.

In each simulation, the Milky Way is initialized at the origin and the LMC is initialized with its observed radial velocity (van der Marel et al. 2002), proper motion (Kallivayalil et al. 2013), and distance (Pietrzyński et al. 2019). They are rewound for 5 Gyr in the presence of each other, including dynamical friction from Jethwa, Erkal & Belokurov (2016), using a kick-drift-kick integrator. At

that point, the stellar halo is injected around the Milky Way as tracer particles and the system is evolved to the present. Mock observations are made on the final snapshot from the location of the Sun, 8.122 kpc from the Milky Way centre (Gravity Collaboration 2018). This stellar halo has all of the salient features as those reported in Garavito-Camargo et al. (2019). Note however, that as our simulation does not contain a live DM halo, additional effects due to emerging DM resonances are not captured. This process is repeated for all six LMC masses. In order to test the stability of our initial conditions, and to compare with the LMC's effect, we also consider a fiducial case where the LMC is not included. In this case, the stellar halo's properties are stable and do not evolve significantly over 5 Gyr.

Fig. 3 shows mock observations of the simulated stellar halo with the effect of a 1.5×10^{11} M$_\odot$ LMC (which roughly matches the LMC mass measured in Erkal et al. 2018) using the same cuts as in Fig. 1. Interestingly, there is a sharp plume-like feature around RA $\sim -20°$ ($\tilde{\Lambda}_\odot \sim 300°$) which matches the observed Pisces Plume shown in Fig. 1. As expected, this overdensity is aligned with the past orbit of the LMC. The dot–dashed green line in the middle-left panel of Fig. 2 shows the distribution of radial velocities in the VVDS footprint, which we approximate with the rectangle, $331° < RA < 341°$, $-0.5° < Dec. < 2°$, and distances, 40 kpc $< D < 110$ kpc. This agrees well with the observed velocity distribution. As in the observations, there is a broad distribution with a shift towards negative velocities. This shift increases with increasing LMC mass. For example, in order to match the observed shift of ~ -57 km s^{-1}, an LMC mass of $\sim 2 \times 10^{11}$ M$_\odot$ is required. Fig. 3 also shows the best-fitting Orphan stream from Erkal et al. (2018) in (red points) which matches the thin, almost vertical, stream visible in the right-hand panel of Fig. 1.

4.2 Conclusions

We have used a sample of RR Lyrae detected in *Gaia* DR2 and PS1 data to trace a long and nearly radial stellar stream, a portion of which had been identified earlier as the Pisces overdensity. Given the stream's stretched appearance in 3D, we have dubbed it the Pisces Plume. The Plume lies at the intersection of the equators of the Sgr and Magellanic Stream coordinate systems. If the Plume is of a Sgr origin then it must be connected to a previously unseen wrap of the Sgr stream, significantly out of the current Sgr plane.
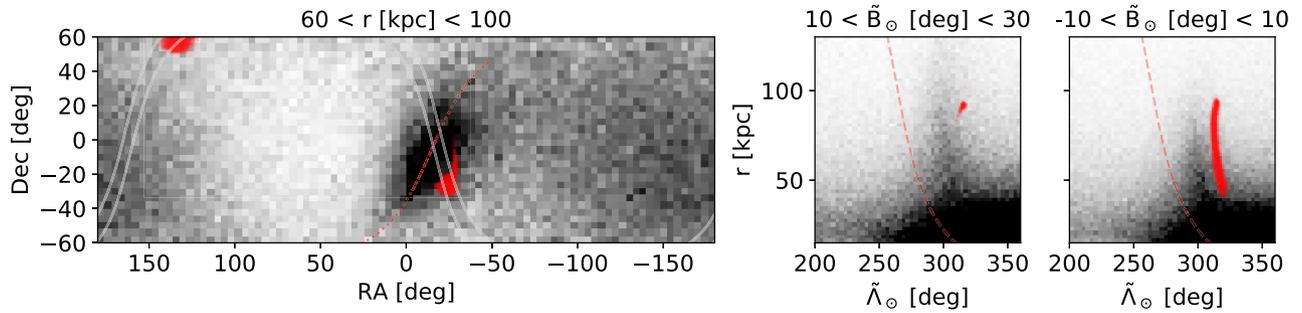
Figure 3. Mock observation of simulated stellar halo perturbed by a 1.5×10^{11} M$_\odot$ LMC with same panels as Fig. 1. *Left:* On-sky density of the stellar halo with Galactocentric distances between 60 and 100 kpc. The dotted red line shows the orbit of the LMC over the past 5 Gyr while the dashed red line shows the portion of the LMC orbit within Galactocentric distances between 60 and 100 kpc. The overdensity occurs in precisely the same part of the sky as the Pisces overdensity (see Fig. 1). The overdensity is aligned with the orbit of the LMC in 3D, following the overall orbit on the sky as well as matching its extent restricted to the same radial range. The grey lines show $\pm 3°$ from the Orphan stream plane and the red points show the best-fitting Orphan stream model from Erkal et al. (2018) with the same Galactocentric distance cuts. *Right:* Distribution of mock stellar halo stars in heliocentric distance versus Sgr's longitude, $\tilde{\Lambda}_\odot$, restricted to two different ranges of Sgr's latitude, $\tilde{B}_\odot$. The dashed red line shows the distance gradient from Nie et al. (2015) and the red points show the best-fitting Orphan stream model from Erkal et al. (2018) subject to the same cuts in $\tilde{B}_\odot$. The overdensity in the wake appears for both latitude ranges, extending out to larger distances at higher latitudes. For $10° < \tilde{B}_\odot < 30°$, the wake has a qualitatively similar distance slope and location in $\tilde{\Lambda}_\odot$ to what is observed (see Fig. 1). At lower latitudes, the wake matches the broad component seen in the data but cannot reproduce the narrow feature. Instead, this feature can be explained by the predicted extension of the Orphan stream. Interestingly, the closest approach between the Orphan stream and the LMC occurs within this extension (see Erkal et al. 2018), suggesting it will be useful for further constraining the LMC mass.

However, the alignment of the Pisces Plume on the sky with the MS equator suggests a possible Magellanic origin.

We have collected VLT FORS2 follow-up spectroscopy of 17 candidate BHB stars detected on the edge of Pisces by Deason et al. (2018) using deep Subaru imaging. Interestingly, radial velocity measurements of candidate Pisces members show a broad dispersion, consistent with the stellar halo, with a shift towards negative values. Guided by previous predictions of the LMC's effect on the Milky Way's stellar halo, (e.g. Erkal et al. 2018; Garavito-Camargo et al. 2019), we simulated the LMC's infall and found that it reproduces well the Pisces Plume's 3D morphology and its radial velocity distribution. This overdensity is the first direct evidence of dynamical friction in action: as the LMC passes through the Milky Way, its gravitational effect induces a wake of stars and dark matter behind it. Since the wake is aligned with the LMC's past orbit, the Pisces Plume offers a way to measure the dynamical friction exerted on the LMC by the Milky Way. This will shed light on the nature of dark matter since dynamical friction depends on its microscopic properties (e.g. Hui et al. 2017). Finally, this interpretation of the Pisces Plume also suggests that the outskirts of the Milky Way are out of equilibrium due to the effect of the LMC on our Galaxy. Indeed, the results of Garavito-Camargo et al. (2019) suggest that we will detect significant velocity offsets over the entire sky, ushering in a new era of disequilibrium modelling.

ACKNOWLEDGEMENTS

REFERENCES

Belokurov V. et al., 2014, MNRAS, 437, 116
Besla G., Kallivayalil N., Hernquist L., Robertson B., Cox T. J., van der Marel R. P., Alcock C., 2007, ApJ, 668, 949
Bird S. A., Xue X.-X., Liu C., Shen J., Flynn C., Yang C., 2019, AJ, 157, 104
Bovy J., 2015, ApJS, 216, 29
Clementini G. et al., 2019, A&A, A60, 37
Clewley L., Warren S. J., Hewett P. C., Norris J. E., Peterson R. C., Evans N. W., 2002, MNRAS, 337, 87
Deason A. J., Belokurov V., Evans N. W., 2011, MNRAS, 416, 2903
Deason A. J., Belokurov V., Koposov S. E., 2018, ApJ, 852, 118
Erkal D. et al., 2018, MNRAS, 481, 3148
Garavito-Camargo N., Besla G., Laporte C. F. P., Johnston K. V., Gómez F. A., Watkins L. L., 2019, preprint (arXiv:e-print)
Gómez F. A., Besla G., Carpintero D. D., Villalobos Á., O'Shea B. W., Bell E. F., 2015, ApJ, 802, 128
Gravity Collaboration, 2018, A&A, 615, L15
Hernitschek N. et al., 2017, ApJ, 850, 96
Holl B. et al., 2018, A&A, 618, A30
Hui L., Ostriker J. P., Tremaine S., Witten E., 2017, Phys. Rev. D, 95, 043541
Iorio G., Belokurov V., 2019, MNRAS, 482, 3868
Jethwa P., Erkal D., Belokurov V., 2016, MNRAS, 461, 2212
Kallivayalil N., van der Marel R. P., Besla G., Anderson J., Alcock C., 2013, ApJ, 764, 161
Kollmeier J. A. et al., 2009, ApJ, 705, L158
Koposov S. E. et al., 2019, MNRAS, 485, 4726
Lancaster L., Koposov S. E., Belokurov V., Evans N. W., Deason A. J., 2019, MNRAS, 486, 378
Laporte C. F. P., Gómez F. A., Besla G., Johnston K. V., Garavito-Camargo N., 2018, MNRAS, 473, 1218
Navarrete C. et al., 2019, MNRAS, 483, 4160
Nidever D. L., Majewski S. R., Butler Burton W., 2008, ApJ, 679, 432
Nie J. D. et al., 2015, ApJ, 810, 153
Peñarrubia J., Gómez F. A., Besla G., Erkal D., Ma Y.-Z., 2016, MNRAS, 456, L54
Pietrzyński G. et al., 2019, Nature, 567, 200

Posti L., Binney J., Nipoti C., Ciotti L., 2015, MNRAS, 447, 3060

Sesar B. et al., 2007, AJ, 134, 2236

Sesar B., Vivas A. K., Duffau S., Ivezić Ž., 2010, ApJ, 717, 133

Sesar B., Hernitschek N., Dierickx M. I. P., Fardal M. A., Rix H.-W., 2017, ApJ, 844, L4

van der Marel R. P., Kallivayalil N., 2014, ApJ, 781, 121

van der Marel R. P., Alves D. R., Hardy E., Suntzeff N. B., 2002, AJ, 124, 2639

Vasiliev E., 2019, MNRAS, 482, 1525

Watkins L. L. et al., 2009, MNRAS, 398, 1757

Xue X.-X. et al., 2011, ApJ, 738, 79

This paper has been typeset from a TEX/LATEX file prepared by the author.